Optical and Quantum Electronics (2024) 56:357
https://doi.org/10.1007/s11082-023-05920-4

Photo-induced single-electron tunnelling based Coulomb staircase effect observed at high applied bias in ZnSe/CdSe core-shell quantum dots

K. C. Handique[1,2] · P. K. Kalita[1] · B. Barman[1] · Hirendra Das[3]

Received: 14 July 2023 / Accepted: 22 November 2023 / Published online: 30 December 2023

Abstract
In this study, ZnSe, CdSe, and their inverse type-I ZnSe/CdSe core-shell quantum dots (QDs) have been synthesized through the chemical bath deposition using polyvinylpyrrolidone (PVP) as a capping agent. Various structural and morphological characterizations were carried out which reveal the cubic zinc blende type structure having spherical shaped core and core-shell QDs nanostructures. The synthesized samples were excited by white light at different intensities in order to investigate their photoinduced current-voltage (*I–V*) characteristics. The Coulomb staircase, a unique quantum mechanical phenomenon, is observed in the *I–V* characteristics of the core-shell QDs when white light interacts with them. A semiempirical two-tunnel junction model for the QDs has been adopted to examine the phenomenon quantitatively. The genesis and nature of this photon-induced unique behavior have been discussed in length. The observed photon-assisted oscillatory Coulomb staircase behavior in the ZnSe/CdSe core-shell QDs is attributed to surface and interface-induced defects that occurred during the synthesis process. The current study focuses primarily on the novel photo-electronic properties of ZnSe/CdSe core-shell QDs, which necessitates a more detailed theoretical investigation to enable the implementation of these materials in next-generation nanoelectronic devices.

Keywords Core-shell QDs · Coulomb blockade · Coulomb staircase · *I–V* characteristics

✉ K. C. Handique
kshirudhandique@gmail.com

✉ P. K. Kalita
pradip.kalita@rgu.ac.in

[1] Department of Physics, Rajiv Gandhi University, Itanagar, Arunachal Pradesh 791112, India

[2] Department of Physics, Jengraimukh College, Majuli, Assam 785105, India

[3] Department of Electronics and Communication Technology, Gauhati University, Guwahati, Assam 781014, India

1 Introduction

Semiconductor QDs have attracted much attention in the past few decades due to its three-dimensional carrier confinement phenomena as well as size and shape-dependent tunable electronic and optical properties (Brus 1984; Handique and Kalita 2020). Growing a thin shell of a wide band gap material over an another semiconductor QD enhances the stability of the structure by passivating the core surface and thus enhancing its luminescence property (Bruchez Jr et al. 1998). Due to its wide range of applications in electronic devices, phosphors, light emitting and photo-detecting devices, solar cells, etc., group II–VI wide bandgap semiconductors have undergone extensive research over the years (Jie et al. 2010; Zhong et al. 2012). Inverse type-I core-shell nanocrystals, with a larger band-gap semiconductor QD as core and narrower band-gap semiconductor as shell material, could alter the electronic properties significantly as the electron and hole are confined in the shell region. If deviation in bandgap of two materials is smaller it boost a great improvement in both charge seperation as well as surface passivation to promote the optoelectronic properties over bare core nanocrystals (Zhong et al. 2005; Ca et al. 2015a, 2015b). Unlike type-I structures, inverse type-I configurations spatially separate electron and hole wave functions, reducing non-radiative recombination and making them promising for next-generation optoelectronic devices (Ca et al. 2015a, 2019). Sabah et al. (2023) prepared highly emissive core-multi-shell (CdSe/CdS/ZnS) QDs (sizes 2–5 nm) and observed a red shift in both the absorption and emission results. Wang and Haque (Zhang et al. 2023) reported the fabrication of ZnSe/ZnS core-shell QDs in silicate glass which shows that the addition of shell material on the core can highly enhance its overall optical properties. Ca et al. (2015b) studied the dependence of emission energy on excitation energy and found an optimal shell thickness and charge separation for chemically synthesized CdS/ZnSe type-II core-shell heterostructures. Tang et al. (2022) have synthesized CdS/ZnS core-shell QDs and observed the temperature dependence of its properties and carrier recombination process for device applications. Das et al. (2021) in 2021 reported the effect of ZnS and PbS shell on the electrical properties of CdS QDs.

Due to their small lattice mismatch, ZnSe/CdSe core-shell QDs exhibit low concentration of defects in the shell and also provide very high photoluminescence (PL) quantum efficiencies, up to 80–90% (Talapin et al. 2004). An important aspect of ZnSe/CdSe core-shell QDs is the influence of the anion at the surface, which results in a substantial band offset in the conduction band, measuring at 0.77 eV. This effect causes the electron wave function to fully extend into the shell region. This phenomenon can be strategically leveraged to modify the optoelectronic properties of these QDs to one's advantage.

Single electron transistor (SET) is a nanoscale device that is sensitive to coulomb oscillatory behavior. Different nanostructures were investigated by the scientific community for the fabrication of SET during the past few years (Aminzadeh et al. 2017; Khademhosseini et al. 2018, 2022). SET is made up of a tiny island with a self-capacitance that is weakly connected to the source and drain contacts through tunnel barriers. At low temperatures and bias voltages, adding an additional electron to the island may cost more energy than the thermal energy, resulting in a blockage of the island's current which is the origin of the oscillatory staircase behavior in the current-voltage characteristics of such devices (Gorter 1951; Fulton and Dolan 1987). With the application of a sweeping external bias voltage, Kalita et al. reported the presence of coulomb oscillations in the *I–V* characteristics of CdS, ZnS, and CdS/ZnS core-shell QDs (Kalita et al.

2023). Several previous studies (Khondaker and Yao 2002; Kuzmin and Likharev 1987; Likharev 1988; Li and Ri 1989) have also reported oscillatory behavior in ultra-small tunnel junctions and nanocomposites.

In the present study, an in-depth investigation is carried out on the photon-induced quantum mechanical properties of ZnSe/CdSe inverse type-I core-shell QDs with the help of its I–V characteristics.

Single electron tunneling (SET) phenomena were used to investigate the observed coulomb staircase behavior (CSB) at high voltages in the photosensitive *I–V* characteristics curve of the core-shell devices. The resistances and capacitances that affect the *I–V* characteristics of such SET devices were calculated using a semi-classical model proposed by Mullen et al. (1988). These findings highlight significant disparities in the photo-induced electrical properties when comparing bare ZnSe QDs with ZnSe/CdSe core-shell QDs. By scrutinizing the conduction mechanisms and the fundamental principles governing their electrical behaviors under distinct illumination conditions, this research may pave the way for new insights into their applications for next-generation nanoelectronic devices.

2 Experimental

ZnSe QDs were synthesized in this research employing zinc acetate ($Zn(CH_3COO)_2 \cdot 2H_2O$, purity 99%) as the zinc ion complex and sodium seleno sulfite (Na_2SeSO_3) as the selenium ion complex. During the synthesis process, PVP is utilized as a capping agent, along with two additional complexing agents, hydrazine hydrate and ammonia. Initially, 3% PVP solution is prepared and by using it zinc ion complex (0.001 M) and selenium complexes are prepared separately. The sodium selenosulphate, which is a complex of selenium ion, is produced by dissolving black selenium powder and sodium sulphite (Na_2SO_3) in the ratio of their respective molarities, which is 1:4. In order to expedite the formation of ZnSe nanocrystals, a small amount of ammonia (3–4 drops) and 10 ml of hydrazine hydrate are added to the Zn ion complex and sodium selenosulphate solutions, respectively. The purpose of hydrazine hydrate in this case is to provide alkalinity to the solution mixture and a homogeneous solution environment for the formation of a complex with Zn^{2+} and to prevent the formation of $ZnSeO_3$ precipitation. Following this, both the ion complexes, i.e., the zinc and selenium, are mixed in equal volumes and stirred for 7 h to achieve the desired light yellow colored ZnSe nanoparticles. The functional groups attached to PVP are expected to bring the overall quantum confinement on the ZnSe nanocrystals. The chemical structure of PVP and the schematic of its mechanism for the encapsulation of ZnSe particles is shown in Fig. 1.

For the synthesis of ZnSe/CdSe core-shell nanocrystals, a part of the initially prepared ZnSe nanoparticle samples is taken on a beaker. Two equimolar solutions of Cd ion complex and Se complex were prepared in the same way as in the case of ZnSe and allowed to fall simultaneously dropwise, very slowly on ZnSe samples to form the growth of shell CdSe on the surface of ZnSe core.

The following are the chemical reactions that take place when ZnSe QDs are synthesized.

$$3Se_3^{2-} + 3N_2H_4 \rightarrow 3Se + 3N_2 + 3H_2O + 6OH^-$$

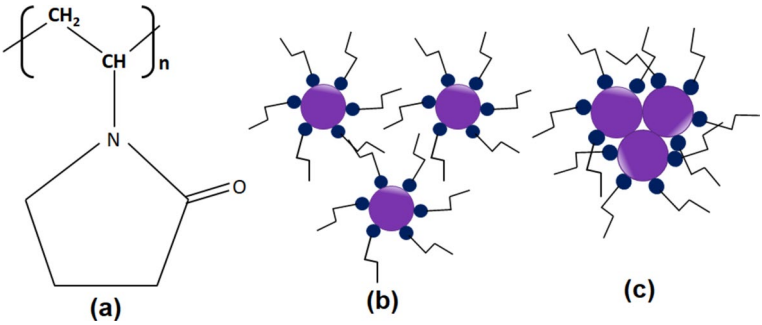

Fig. 1 Structure of PVP (**a**), a schematic showing the mechanism for the encapsulation of PVP on ZnSe nanoparticles: optimum coverage (**b**), complete coverage (**c**)

$$3\mathrm{Se} + 6\mathrm{OH}^- \rightarrow 2\mathrm{Se}^{2-} + \mathrm{SeO32} + 3\mathrm{H_2O}$$

$$2\mathrm{Se}^{2-} + 2\mathrm{Zn}\left(\mathrm{NH_3}\right)_4^{2+} \rightarrow 2\mathrm{ZnSe} + 8\mathrm{NH_3}$$

3 Results and data analysis

Various characterization techniques were carried out to investigate the structural, optical, electrical, and chemical properties of the as synthesized core-shell samples. The X-ray diffraction (XRD) patterns (with JCPDS number) of CdSe, ZnSe and ZnSe/CdSe core-shell QDs were carried out within the range of 2θ from 20° to 80° using Ultima-IV X-Ray diffractometer with *CuKα* radiation ($\lambda = 1.54$ Å) as shown in Fig. 2. The diffraction pattern for ZnSe reflects cubic nature with five distinct and broad peaks for planes (111), (220), (311), (400), and (331) at 2θ positions of 27.35°, 45.53°, 53.86°, 66.41°, and 73.48° respectively (JCPDS file no. 37-1463). The shell material CdSe also possesses cubic structure with distinct peaks for planes (111), (220), and (311) at 2θ values of 25.64°, 42.49° and 49.86° respectively (JCPDS card no 19-0191). The formation of CdSe shell over ZnSe core in core/shell sample is confirmed from the the relative variation in intensity. For both the core and shell materials, the intensity of XRD peaks are satisfactorily high at lower angles which indicates good crystallinity. Strong quantum confinements and the possible presence of strain and other elastic parameters are indicated by the presence of broadened diffraction peaks in the samples.

For ZnSe/CdSe samples, the presence of diffraction peaks of crystal plans from both core and shell material indicates the formation of core-shell structure (Zhong et al. 2005). The crystallite sizes (D) of the prepared samples are calculated using the Debye Scherrer formula (Patterson 1939; Mustapha et al. 2019; Bokuniaeva and Vorokh 2019)

$$D = 0.94\lambda/\beta cos\theta \tag{1}$$

Where *'D'* denotes the crystallite size, '*k*' has a value of 0.94, λ = 1.54 Å (X-ray wavelength), β is FWHM in radian, and θ is Bragg's angle corresponding to the diffracting planes. The crystallite sizes for the core, shell and core-shell are presented in Table 1. The

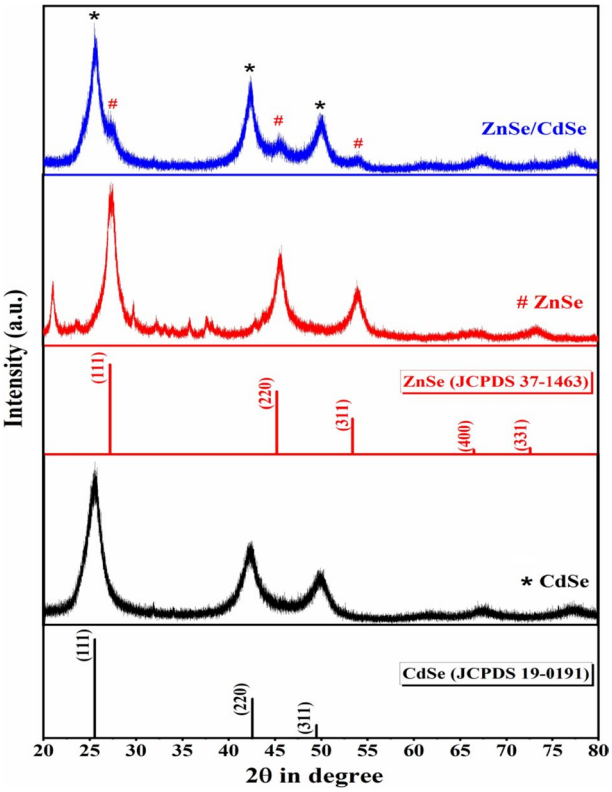

Fig. 2 X-ray diffraction spectra of ZnSe, CdSe and ZnSe/CdSe QDs.

Table 1 Structural parameters of the synthesized ZnSe, CdSe and ZnSe/CdSe QDs.

Samples	2θ	hkl	d_{hkl} (nm)	Structure	D (nm) (from Scherrer plot)
ZnSe	27.35	111	0.3181	Cubic	14.4
	45.54	220	0.1943		
	53.86	311	0.1661		
CdSe	25.64	111	0.347	Cubic	13.33
	42.49	220	0.2125		
	49.86	311	0.1826		
ZnSe/CdSe	26.77	111	0.3327	Cubic	14.54
	51.3	220	0.1778		
	61.8	311	0.1499		

crystallite size of the core is slightly increasing after shelling which is the usual behavior of core shell materials. The interplanar spacing *'d'* of the diffracting planes are calculated using Eq. (2) (Xiong et al. 2021; Tang et al. 2019)

$$2dsin\theta = n\lambda \tag{2}$$

The high-resolution TEM images are shown in Fig. 3. The particles are of nearly spherical shaped and are distributed uniformly within the sample for both the core and core-shell

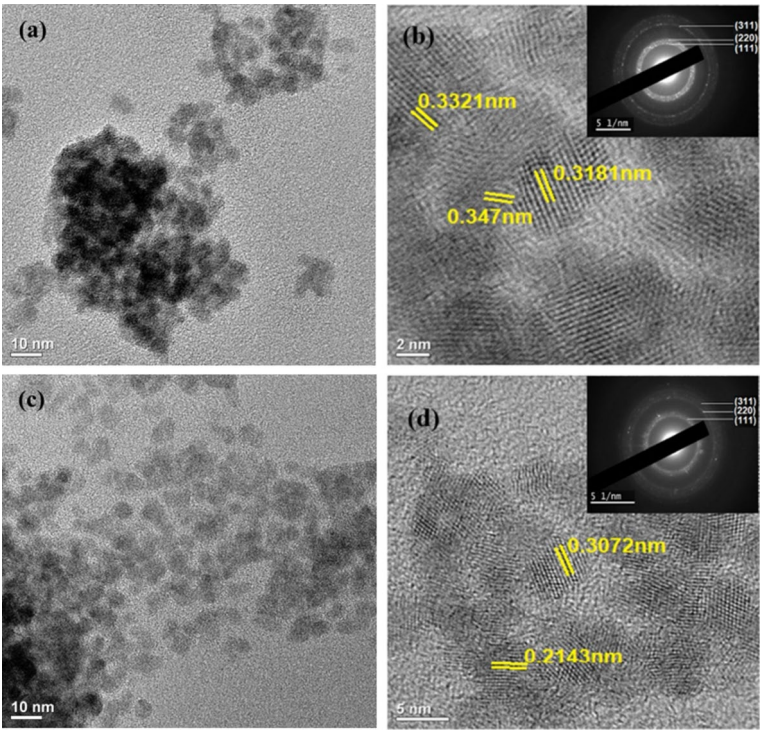

Fig. 3 HRTEM images; particle distribution of ZnSe (**a**) and ZnSe/CdSe (**c**); lattice fringes and SAED spectra of ZnSe (**b**) and ZnSe/CdSe (**d**)

as seen from Fig. 3a and c. The lattice fringes of both the core and core-shell are shown in Fig. 3b and d respectively. The fringe width of the crystallites matches well with the results found from XRD measurements. In the case of core ZnSe, the *d* values of various crystal planes are calculated as 0.3321 nm, 0.3181 and 0.347 nm with the help of image J software which corresponds to (111) plane while in the case of core-shell ZnSe/CdSe the *d* values are 0.3072 nm and 0.2143 nm which corresponds to (111) and (311) planes. The SAED pattern of the core and core-shell samples are shown in the inset of respective figures which can be associated with the three distinct (111), (220) and (311) planes that agrees with XRD results.

The surface morphology and elemental analysis of the prepared samples is carried out with the help of a Zeiss Field emission scanning electron microscope. Figure 4A–C shows the FESEM images of uniformly distributed spherical-shaped particles of the ZnSe core, CdSe shell and ZnSe-CdSe core-shell samples respectively. The particle sizes of the core-shell samples are relatively bigger than the core and shell sizes separately that may be attributed to the formation of core-shell structure and validate the XRD results presented in Table 1.

The energy dispersive X-ray spectroscopy (EDS) for ZnSe core, CdSe shell and ZnSe/CdSe core-shell QDs are carried out to study the elemental composition of the synthesized samples and shown in Fig. 4D–F. The presence of various elements in weight (%) is shown in the Fig. 4D–F. Figure 4D shows the presence of zinc and selenium with a little impurity

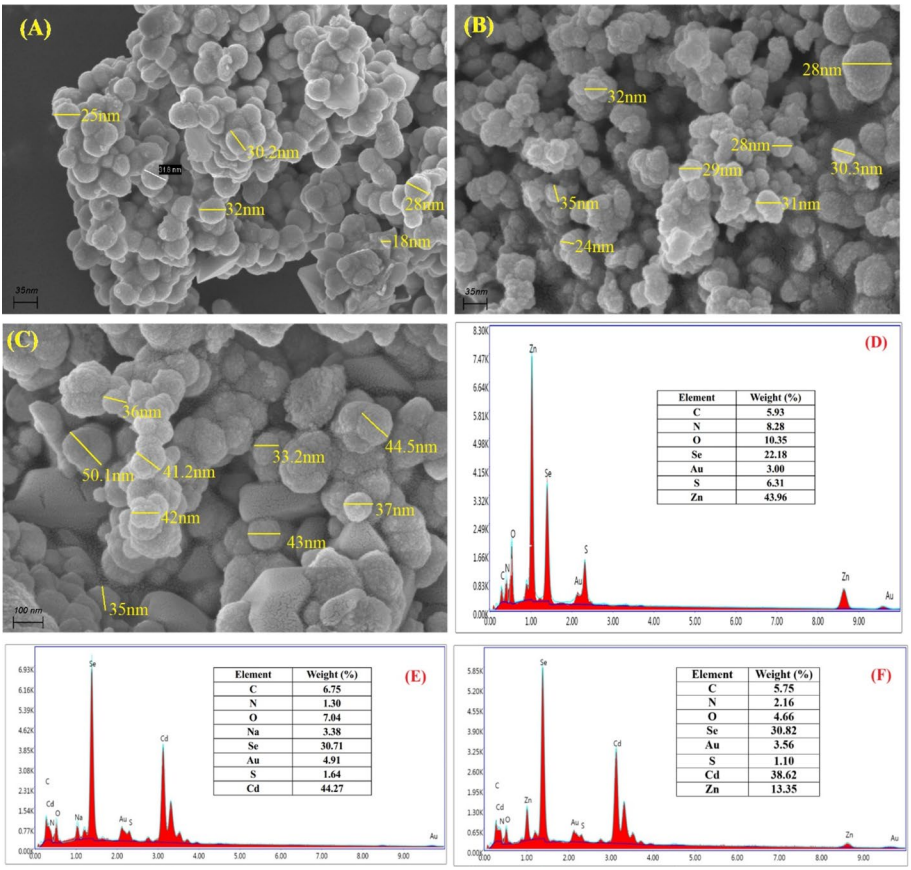

Fig. 4 FESEM micrograph of **A** ZnSe core, **B** CdSe Shell, **C** ZnSe/CdSe Core-shell samples. EDS spectra of **D** ZnSe, **E** CdSe and **F** ZnSe/CdSe QDs with weight% of elements

of Au, O, and S. Similarly, Fig. 4E shows the presence of Cd and Se. In the case of the core-shell sample, the presence of both Cd and Zn along with Se can be seen in the EDS spectra (Fig. 4F). The weight (%) of cadmium is more than zinc that also validate the formation of ZnSe/CdSe core shell QD.

3.1 Optical analysis

The UV-visible spectra of the synthesized samples are taken with the help of UV-Vis spectrometer (Agilent Cary eclipse spectrometer) in the range of 200–800 nm and shown in Fig. 5a. The absorbance spectra of the samples are found to be blue-shifted compared to their bulk counterparts (Hong et al. 2020; Akter et al. 2020) indicating quantum confinement. The absorption edge of pristine ZnSe is found to be at 266 nm which is red-shifted to 440 nm after core-shell formation due to the increase of particle size. The estimated band gap from Tauc's equation for ZnSe and CdSe is around ~4.5 eV and 3.7 eV respectively. For ZnSe/CdSe core-shell QDs the band-gap is estimated to be 3.6 eV.

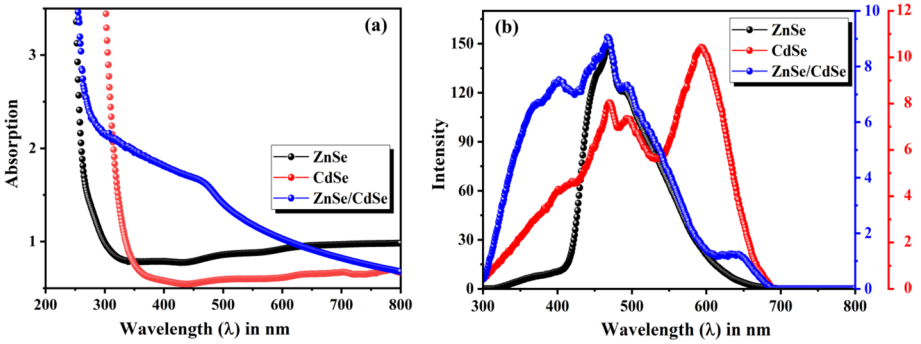

Fig. 5 **a** UV-Visible and **b** PL spectra of ZnSe, CdSe and ZnSe/CdSe QDs

The PL spectroscopy of the as-synthesized samples are recorded using a Cary Eclipse spectrometer is shown in Fig. 5b. The figure clearly illustrates distinct emission characteristics for ZnSe QDs with a sharp peak centered around 470 nm, while CdSe emits at 594 nm. For ZnSe, another peak around 498 nm is observed, likely to be originating from surface-induced near-bandgap emission. PL shows a sharp reduction of intensity for core-shell nanostructures over core which signifies its suitability in photoconductive application. The significant increase in the Full Width at Half Maximum (FWHM) of ZnSe-CdSe over that of ZnSe, is an another aspect that makes it a promising candidate for applications in photoelectronic multicolor/white colour light-emitting diodes (LEDs).

3.2 DC current-voltage (*I–V*) characteristics

Planar devices were fabricated using the synthesized samples to study the *I–V* characteristics. A schematic diagram of the fabricated device is shown in Fig. 6a. Thin films of ZnSe (core) and ZnSe/CdSe (core-shell) QDs were deposited on glass substrate. Upon the film two Ag electrodes (Conducting silver paste was purchased from Sigma) were pasted keeping a gap of 1 mm. The electrodes were connected to Kitheley sourcemeter (2450) for photoelectronic measurements in the dark and under light of different intensities.

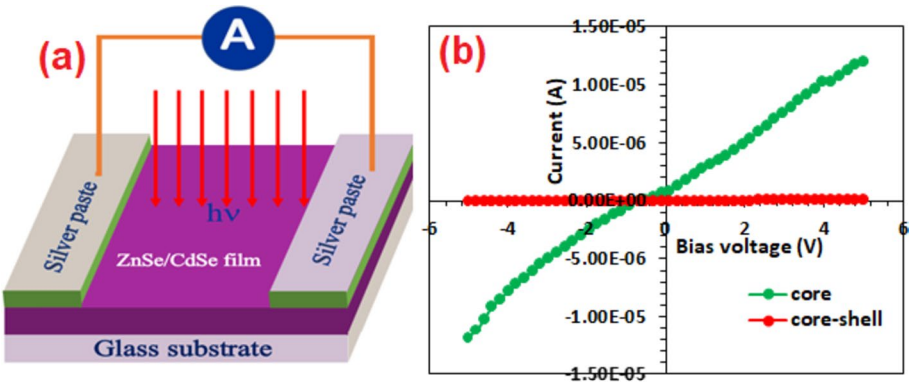

Fig. 6 Planar geometry with film (**a**), *I–V* curve of ZnSe (core) and ZnSe/CdSe (core-shell) (**b**)

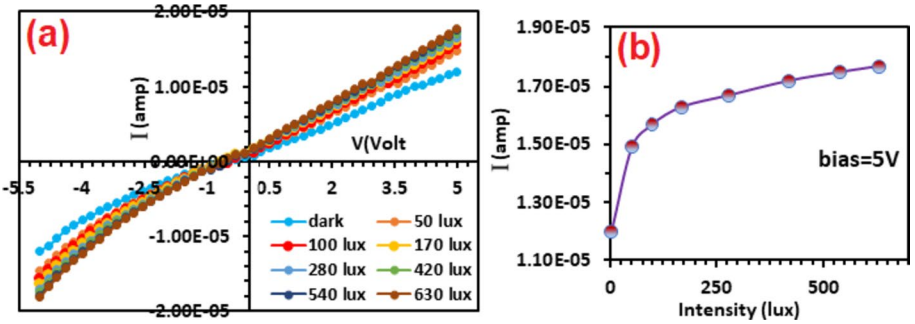

Fig. 7 *I–V* characteristics of ZnSe QDs (**a**); Photocurrent vs. light intensity characteristics (**b**)

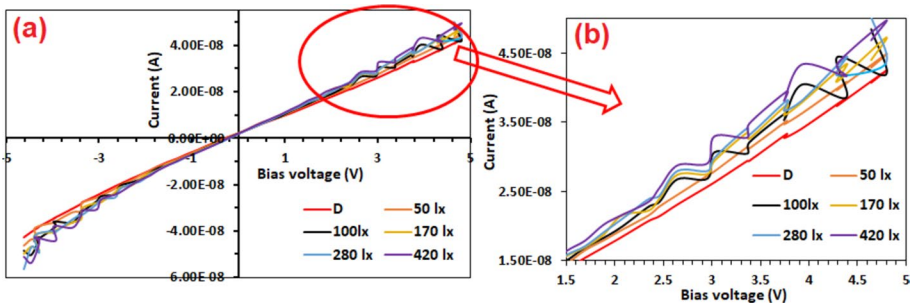

Fig. 8 *I–V* characteristics of ZnSe/CdSe core-shell QDs (**a**); staircase behaviour at high bias (**b**)

A sweeping voltage of − 5 V to + 5 V was applied across the device terminals fabricated with core and core-shell NPs to record the *I–V* characteristics shown in Fig. 6b. It can be observed from the figure that ZnSe/CdSe core-shell QD device exhibits significantly less current compared to the ZnSe core, consistent with inverse type-I core-shell structures (Kalita et al.). The surface defects introduced by shelling are expected to act as non radiative centres at the inteface and control the recombination kinetics. Defects either acts as traps or recombination centres; as the density of recombination centres enhanced, it eventually reduces the current mainly due to the loss of electrons and holes.

The photoresponse properties of the ZnSe core and ZnSe/CdSe core-shell QDs were investigated under different intensities of white light at room temperature. The ZnSe core has shown an ohmic *I–V* characteristics where current increases with the increase of incident light intensity as shown in Fig. 7a. The figure clearly shows that ZnSe QDs have a zero bias current which increases slowly with the increase of light intensity. This may be due to the generation of free charge carriers at the electrode-semiconductor junction as a result of thermal agitation.

The maximum photocurrent vs. light intensity characteristics of the as-synthesized ZnSe QDs at a constant bias voltage of 5 V is shown in Fig. 7b where a zero-bias current of 12 μA can be observed. The photocurrent increases linearly with the increase of light intensity up to 170 lx and then follow a sublinear behaviour upto applied 630 lx. The sublinear behaviour is attributed to changeover of more no of traps into recombination centres.

The *I–V* characteristics of ZnSe/CdSe core-shell QDs are shown in Fig. 8a which exhibit a unique coulomb staircase and coulomb blockade behavior. From the figure, it is evident that without any incident light, the current-voltage relationship is almost linear (red curve, Fig. 8a).

Figure 8b shows a prominent staircase behavior at the high bias region. Similar coulomb staircase structure was also reported by Bekenstein et al. in Cu_2S/Ru semiconductor/metal cage NPs (Bekenstein et al. 2012). For a clear and better realization of these effects, the *I–V* graphs of the ZnSe/CdSe core-shell QDs are plotted separately as shown in Fig. 9. It can be observed that in the absence of light, the current-voltage relationship is ohmic in nature. When the device is exposed to incident light, a staircase structure is emerged which becomes more prominent as the light intensity increases. This unique behavior basically occurs in a double-barrier single-electron tunneling system with asymmetric barriers (Grabert and Devoret 2013).

As the intensity of incident light increases, greater number of charge carriers will be generated and some sub-bands will be formed where the electrons and holes will reside. The current is zero when the charging energy changes from $-e^2/2$ C to $+e^2/2$ C because the electron is locked. Nevertheless, if the charging energy is less than $-e^2/2$ C or greater than $+e^2/2$ C, the electron will cross the coulomb barrier resulting in a non-zero tunneling current. In this case, towards the low voltage regions in the range of − 2 to 2 V, the I–V curves are almost ohmic in nature, which is called zero-bias conductance. The Coulomb staircase effect becomes prominent only outside of this range in both positive and negative directions. Khondaker et al. also reported similar behavior in thiol-coated gold NPs that showed Coulomb staircase pattern in high-voltage regions (Khondaker and Yao 2002).

The corresponding dI/dV vs. V and d^2I/d^2V vs. V tunneling spectra are plotted and shown in Fig. 10 which indicates the transition from a state of finite tunneling density of states (DOS) at zero bias in the low voltage region to a state of coulomb staircase and coulomb blockade for the ZnSe/CdSe core-shell QDs at different light intensities. The average energetic gap between successive peaks may easily be used to calculate the single electron charging energy, E_C, since each peak in the dI/dV − V spectrum represents a change of one in the number of surplus electrons on the quantum dot.

The coulomb staircase phenomena are caused by charge quantization in ZnSe/CdSe core-shell QDs which are capable of quantum charge fluctuations when single electron transmission occurs. This oscillatory staircase behavior in the high voltage region in the

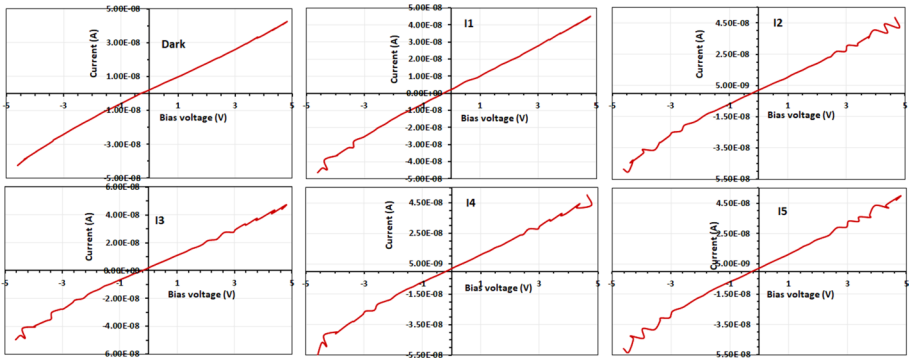

Fig. 9 *I–V* characteristics of ZnSe/CdSe core-shell QDs at different light intensities

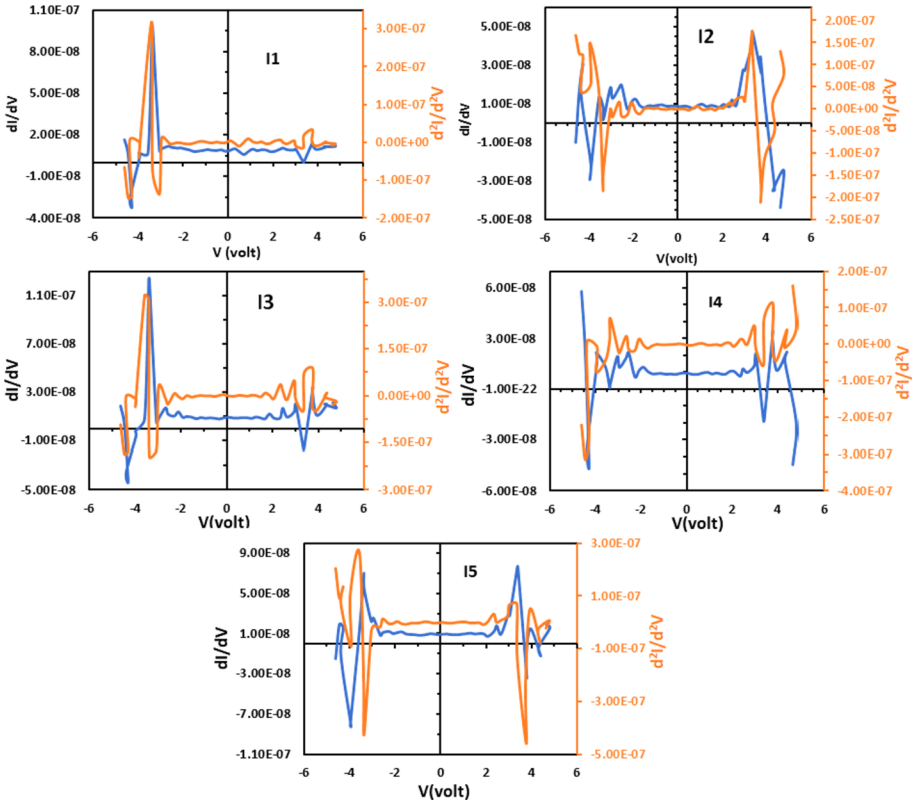

Fig. 10 The first and second derivatives of I–V curves for core-shell QDs at different light intensities

photo-response properties of core-shell QDs arises due to electron-electron interaction. Due to the significant size quantization of the core-shell QDs, quantum corrections were caused by them. At high bias, these quantum corrections were further modified to include nonlinear corrections caused by the partial densities of states filled separately by the two contacts (Muralidharan et al. 2007).

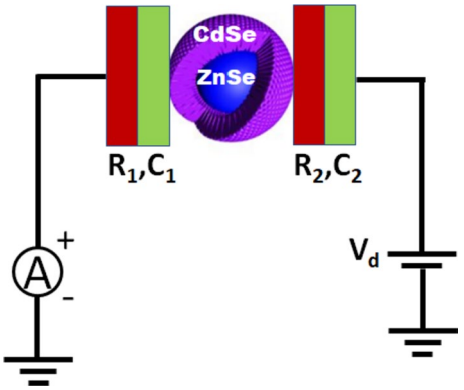

Fig. 11 Schematic diagram of two-tunnel junction model of core-shell QD device

A schematic of a two-tunnel junction model of the ZnSe/CdSe core-shell QD device is given in Fig. 11. The two capacitors C_1 and C_2 are proposed to be formed by a metal-insulator-metal junction that, when charged by an electron, creates a voltage $V_c = e/C$ across the junction, where '*e*' is the electron charge and C is the junction capacitance. These capacitors and resistors arise from the interface of defect-induced surface of the core-shell structure and electrode in this instance. The conditions are typically $R_1 << R_2$ and $C_1 << C_2$ in order to achieve a staircase pattern in the I–V characteristics. Mullen et al. (1988) demonstrated that the values of C_1, R_1, C_2, and R_2 can control the *I–V* characteristics of these types of devices.

The voltage drops across C_1 and C_2 are given by

$$V_1 = \frac{C_2V - \delta Q}{C_1 + C_2} \text{ and } V_2 = \frac{C_1V - \delta Q}{C_1 + C_2} \tag{5}$$

Where, δQ is charge of electrons in the coulomb island. An increase of external voltage V raises δQ by one electron, resulting in a spike in V_2 by $e/(C_1+C_2)$ which increases the current by

$$\Delta I = \frac{\Delta V_2}{R_2} = \frac{e}{R_2\left(C_1 + C_2\right)} \tag{6}$$

The values of ΔV and ΔI for the fabricated devices at various lighting conditions are taken from Fig. 10 and the remaining device parameters (R_2, C_2, C, and C_1) are calculated using the above relations and presented in Table 2. For the device I1(illuminated with 50 lx), $\Delta V = 337$ mV and $\Delta I = 5.9$ nA, $R = R_1 + R_2 = 0.057 \times 10^9$ Ω, and $C_2 = 4.747 \times 10^{-19}$ F. If we remind the previous assumption $R_2 >> R_1$ then $R_2 \sim R = 0.057 \times 10^9$ Ω which can further be utilized to calculate $C = C_1 + C_2 = 4.757 \times 10^{-19}$ F and hence $C_1 = 0.01 \times 10^{-19}$ F. Similarly, for different intensities of incident light, the device parameters were calculated and given in Table 2. The accuracy of basic current and voltage measurement is 0.012%.

The estimated values are quite in agreement with the reported values which signify that the present study may show useful direction in the development of future photi-conductive single electron transistor. More studies are desirable to explore the true cause of these extraordinary photo-induced tunneling behaviors in ZnSe/CdSe core-shell QD devices, which would be a huge advancement in this field from an application standpoint.

Table 2 Calculated device parameters of ZnSe/CdSe core-shell device at different intensities of light

Intensity (lux)	ΔV (mV)	ΔI (nA)	R_2 (Ω)	C_2 (F)	$C = C_1 + C_2$ (F)	C_1 (F)
I1(50)	337	5.9	0.057×10^9	4.747×10^{-19}	4.757×10^{-19}	0.01×10^{-19}
I2(100)	381	3.9	0.097×10^9	4.199×10^{-19}	4.229×10^{-19}	0.03×10^{-19}
I3(170)	575	5.9	0.097×10^9	2.782×10^{-19}	2.795×10^{-19}	0.013×10^{-19}
I4(280)	299	4.1	0.072×10^9	5.351×10^{-19}	5.42×10^{-19}	0.069×10^{-19}
I5(420)	381	4.2	0.090×10^9	4.199×10^{-19}	4.232×10^{-19}	0.033×10^{-19}

4 Conclusion

PVP-capped ZnSe, CdSe, and ZnSe/CdSe core-shell quantum dots have been synthesized using the chemical bath deposition method. Using XRD, FESEM, and HRTEM analysis, the samples' structural and morphological characteristics were investigated. The cubic structure of the core and shell, with its three different planes (111), (220), and (311) are observed. In the core-shell XRD, the diffraction peaks of the core and shell are both present and the peak intensity in shell become more than core that confirms the formation of ZnSe/CdSe core-shell QDs. The cubic structure, crystallite size, and interplanar distance between the crystal planes are visible in HRTEM images, which are in agreement with the XRD results. The samples' spherical shape and homogenous particle distribution are shown in FESEM pictures. Optical analysis, including absorption and PL spectroscopy, indicated quantum confinement effects in quantum dots, leading to blue-shifted absorption edges and unique emission properties. The bandgap shows a decrease from 4.5 nm (core) and 3.7 nm (shell) to 3.6 nm for core-shell structure that may be attributed to the formation of the core shell with increased particle size. PL spectroscopy unveiled intriguing emission characteristics, with ZnSe displaying a sharp peak at 470 nm, CdSe at 594 nm and the core-shell at 475 nm, showcasing the impact of core-shell structure on the emission properties. The substantial increase in full width at half maximum (FWHM) for ZnSe/CdSe core-shell suggests its potential for application in photoelectronic multicolor light emitting devices. In order to obtain the *I–V* characteristics of the devices, planar geometry devices were fabricated using the as synthesized ZnSe core, CdSe shell and ZnSe/CdSe core-shell QDs. The I–V characteristics of the core-shell structure exhibit significantly reduced current compared to the core which is consistent with defect controlled core-shell structure. This reduction in current is attributed to non radiative recombination kinetics of electron and hole at the surface of QDs. the Photo-response properties of both core and core-shell QDs have been investigated in the range -5 to 5 V in response to the incident white light of different intensities. It shows a typical ohmic nature in ZnSe QD and the photocurrent increases from 1.2×10^{-5} to 1.78×10^{-5} A with incident light intensity from zero to 630 lx. On the other hand, the Coulomb staircase behaviour has been observed in the photo-response of ZnSe/CdSe in high applied bias which is explained on the basis of quantum mechanical single-electron tunneling effect. This unique behavior is assumed to be originated due to the surface and interface effects along with the band alignment of core-shell QDs. A semi-empirical two-tunnel junction model for QD devices was used to analyze and justify the oscillatory coulomb staircase behavior which may provide valuable insights into the mechanisms governing these behaviours, shedding light on the roles of capacitance and resistance parameters of the device. The present study thus shows an ample scope for further research in this direction for the development of photo-induced single electron transistor and other photo-electronic devices.

Acknowledgements The authors sincerely thank CIF, IIT Guwahati, Department of Chemistry and Department of Physics, Rajiv Gandhi University for providing necessary instrumental facilities.

Author contributions KCH have done the experimental work and prepared the manuscript, PKK and HD have reviewed the manuscript and BB contributed to the methodology of the work. All authors have reviewed the manuscript.

Funding Not applicable.

Declarations

Conflict of interest The authors have no conflict of interest to disclose.

References

Akter, M., Khan, M.N.I., Mamur, H., Bhuiyan, M.R.A.: Synthesis and characterisation of CdSe QDs by using a chemical solution route. Micro Nano Lett **15**(5), 287–290 (2020). https://doi.org/10.1049/mnl.2019.0200

Aminzadeh, H., Dashti, M.A., Miralaei, M.: Nano-scale silicon quantum dot-based single-electron transistors and their application to design of analog-to-digital convertors at room temperature. J. Circuits Syst. Comput. **26**(12), 1750201 (2017). https://doi.org/10.1142/S0218126617502012

Bekenstein, Y., Vinokurov, K., Banin, U., Millo, O.: Electronic properties of hybrid Cu2S/Ru semiconductor/metallic-cage nanoparticles. Nanotechnology **23**, 505710 (2012). https://doi.org/10.1088/0957-4484/23/50/505710

Bokuniaeva, A., Vorokh, A.: Estimation of particle size using the Debye equation and the Scherrer formula for polyphasic TiO2 powder. In: Paper read at journal of physics: Conference series (2019). https://doi.org/10.1088/1742-6596/1410/1/012057

Bruchez Jr, M., Moronne, M., Gin, P., Weiss, S., Alivisatos, A.P.: Semiconductor nanocrystals as fluorescent biological labels. Science **281**(5385), 2013–2016 (1998)

Brus, L.E.: Electron–electron and electron-hole interactions in small semiconductor crystallites: the size dependence of the lowest excited electronic state. J. Chem. Phys. **80**(9), 4403–4409 (1984). https://doi.org/10.1063/1.447218

Ca, N.X., Lien, V., Nghia, N., Chi, T.: Tunable luminescent emission characterization of type-I and type-II systems in CdS–ZnSe core–shell nanoparticles: Raman and photoluminescence study. Nanotechnology **26**(44), 445701 (2015a). https://doi.org/10.1088/0957-4484/26/44/445701

Ca, N.X., Lien, V., Nghia, N., Chi, T., Phan, T.: Type-II CdS/ZnSe core/shell heterostructures: UV–vis absorption, photoluminescence and Raman scattering studies. Mater. Sci. Eng.: B **200**, 107–116 (2015b). https://doi.org/10.1016/j.mseb.2015.07.003

Ca, N., Hien, N., Luyen, N., Lien, V., Thanh, L., Do, P., Bau, N., Pham, T.: Photoluminescence properties of CdTe/CdTeSe/CdSe core/alloyed/shell type-II quantum dots. J. Alloys Compd. **787**, 823–830 (2019). https://doi.org/10.1016/j.jallcom.2019.02.139

Das, H., Xu, Q., Datta, P.: Effect of ZnS and PbS shell on mem-behavior of CdS quantum dots. J. Mater. Sci.: Mater. Electron. **32**(6), 7049–7060 (2021). https://doi.org/10.1007/s10854-021-05415-6

Fulton, T.A., Dolan, G.J.: Observation of single-electron charging effects in small tunnel junctions. Phys. Rev. Lett. **59**(1), 109–112 (1987). https://doi.org/10.1103/PhysRevLett.59.109

Gorter, C.: A possible explanation of the increase of the electrical resistance of thin metal films at low temperatures and small field strengths. Physica **17**, 777–780 (1951). https://doi.org/10.1016/0031-8914(51)90098-5

Grabert, H., Devoret, M.H.: Single Charge Tunneling: Coulomb Blockade Phenomena in Nanostructures, vol. 294. Springer Science & Business Media, France (2013)

Handique, K., Kalita, P.: Effects of cadmium ion concentration on the optical and photo-response properties of CdSe/PVP nanocomposites for white light sensing application. Appl. Phys. A **126**, 1–12 (2020). https://doi.org/10.1007/s00339-020-03934-3

Hong, H.S., Kim, M.-S., Byun, E.K., Lee, Y.L.: Facile synthesis and characterization of zinc selenide nanoparticles in aqueous solution at room temperature. J. Cryst. Growth **535**, 125523 (2020). https://doi.org/10.1016/j.jcrysgro.2020.125523

Jie, J., Zhang, W., Bello, I., Lee, C.-S., Lee, S.-T.: One-dimensional II–VI nanostructures: synthesis, properties and optoelectronic applications. Nano Today **5**(4), 313–336 (2010). https://doi.org/10.1016/j.nantod.2010.06.009

Kalita, P.K., Nanung, Y., Das, H.: Shell induced optical properties and Coulomb-blockade oscillation in CdS/ZnS core–shell quantum dots. Phys. Scr. **98**(2), 025820 (2023). https://doi.org/10.1088/1402-4896/acb40a

Khademhosseini, V., Dideban, D., Ahmadi, M., Ismail, R., Heidari, H.: Single electron transistor scheme based on multiple quantum dot islands: carbon nanotube and fullerene. ECS J. Solid State Sci. Technol. **7**(10), M145–M152 (2018). https://doi.org/10.1149/2.0081810jss

Khademhosseini, V., Dideban, D., Ahmadi, M.T., Heidari, H.: Schemes for single electron transistor based on double quantum dot islands utilizing a graphene nanoscroll, carbon nanotube and fullerene. Molecules **27**(1), 301 (2022). https://doi.org/10.1149/2.0081810jss

Khondaker, S.I., Yao, Z.: Fabrication of nanometer-spaced electrodes using gold nanoparticles. Appl. Phys. Lett. **81**, 4613–4615 (2002). https://doi.org/10.1063/1.1528285

Kuzmin, L., Likharev, K.: Direct experimental observation of discrete correlated single-electron tunneling. Jetp Lett. **45**(8), 495–497 (1987)

Li, G., Ri, S.: Coulomb oscillations of the conductance in a laterally confined heterostructure. J. Phys. Condens. Matter **1**, 5811–5815 (1989)

Likharev, K.K.: Correlated discrete transfer of single electrons in ultrasmall tunnel junctions. IBM J. Res. Dev. **32**(1), 144–158 (1988). https://doi.org/10.1147/rd.321.0144

Mullen, K., Ben-Jacob, E., Jaklevic, R., Schuss, Z.: I–V characteristics of coupled ultrasmall-capacitance normal tunnel junctions. Phys. Rev. B **37**(1), 98–105 (1988). https://doi.org/10.1103/PhysRevB.37.98

Muralidharan, B., Ghosh, A.W., Pati, S.K., Datta, S.: Theory of high bias coulomb blockade in ultrashort molecules. IEEE Trans. Nanotechnol. **6**, 536–544 (2007). https://doi.org/10.1109/TNANO.2007.898605

Mustapha, S., Ndamitso, M., Abdulkareem, A., Tijani, J., Shuaib, D., Mohammed, A., Sumaila, A.: Comparative study of crystallite size using Williamson-Hall and Debye-Scherrer plots for ZnO nanoparticles. Adv. Nat. Sci.: Nanosci. Nanotechnol. **10**(4), 045013 (2019). https://doi.org/10.1088/2043-6254/ab52f7

Patterson, A.: The Scherrer formula for X-ray particle size determination. Phys. Rev. **56**(10), 978–982 (1939). https://doi.org/10.1103/PhysRev.56.978

Sabah, A., Shafaqat, I., Naifar, A., Albalawi, H., Alqahtani, M.S., Ashiq, M., Shabbir, S.A.: Investigation of band parameters and electrochemical analysis of multi core-shell CdSe/CdS/ZnS quantum dots. Opt. Mater. **142**, 114065 (2023). https://doi.org/10.1016/j.optmat.2023.114065

Talapin, D.V., Mekis, I., Götzinger, S., Kornowski, A., Benson, O., Weller, H.: CdSe/CdS/ZnS and CdSe/ZnSe/ZnS core–shell–shell nanocrystals. J. Phys. Chem. B **108**(49), 18826–18831 (2004). https://doi.org/10.1021/jp046481g

Tang, B., Zhou, J., Fang, G., Liu, F., Zhu, C., Wang, C., Pan, A., Liang, S.: Engineering the interplanar spacing of ammonium vanadates as a high-performance aqueous zinc-ion Battery cathode. J. Mater. Chem. A **7**(3), 940–945 (2019). https://doi.org/10.1039/C8TA09338E

Tang, L., Zhang, Y., Liao, C., Guo, Y., Lu, Y., Xia, Y., Liu, Y.: Temperature-dependent photoluminescence of CdS/ZnS Core/Shell Quantum Dots for temperature sensors. Sensors **22**(22), 8993 (2022). https://doi.org/10.3390/s22228993

Xiong, K., Guo, J., Shen, K., Ling, R., Cai, S., Sun, X., Zheng, C.: Few-layered MoS2 with expanded interplanar spacing strongly encapsulated inside compact carbon spheres by C–S interaction as ultra-stable sodium-ion batteries anode. J. Alloys Compd. **858**, 157675 (2021). https://doi.org/10.1016/j.jallcom.2020.157675

Zhang, J., Zhang, Z., Zhang, S., Wang, J., Han, J.: Efficient photoluminescence from Cu2 + doped ZnSe/ZnS core-shell quantum dots in silicate glass. J. Non-Cryst. Solids **606**, 122225 (2023). https://doi.org/10.1016/j.jnoncrysol.2023.122225

Zhong, X., Xie, R., Zhang, Y., Basche, T., Knoll, W.: High-quality violet-to red-emitting ZnSe/CdSe core/shell nanocrystals. Chem. Mater. **17**, 4038–4042 (2005). https://doi.org/10.1049/mnl.2019.0200

Zhong, H., Bai, Z., Zou, B.: Tuning the luminescence properties of colloidal I–III–VI semiconductor nanocrystals for optoelectronics and biotechnology applications. J. Phys. Chem. Lett. **3**(21), 3167–3175 (2012). https://doi.org/10.1021/jz301345x